JUN 19 1996

SANDIA REPORT

SAND96–1367 • UC–910
Unlimited Release
Printed June 1996

RECEIVED
JUN 28 1996
OSTI

Near Perfect Optics

R. Goeke, A. V. Farnsworth, C. C. Neumann
W. C. Sweatt, M. E. Warren, J. W. Weed

Prepared by
Sandia National Laboratories
Albuquerque, New Mexico 87185 and Livermore, California 94550
for the United States Department of Energy
under Contract DE-AC04-94AL85000

Approved for public release; distribution is unlimited.

MASTER

DISTRIBUTION OF THIS DOCUMENT IS UNLIMITED

Issued by Sandia National Laboratories, operated for the United States Department of Energy by Sandia Corporation.

NOTICE: This report was prepared as an account of work sponsored by an agency of the United States Government. Neither the United States Government nor any agency thereof, nor any of their employees, nor any of their contractors, subcontractors, or their employees, makes any warranty, express or implied, or assumes any legal liability or responsibility for the accuracy, completeness, or usefulness of any information, apparatus, product, or process disclosed, or represents that its use would not infringe privately owned rights. Reference herein to any specific commercial product, process, or service by trade name, trademark, manufacturer, or otherwise, does not necessarily constitute or imply its endorsement, recommendation, or favoring by the United States Government, any agency thereof or any of their contractors or subcontractors. The views and opinions expressed herein do not necessarily state or reflect those of the United States Government, any agency thereof or any of their contractors.

Printed in the United States of America. This report has been reproduced directly from the best available copy.

Available to DOE and DOE contractors from
Office of Scientific and Technical Information
PO Box 62
Oak Ridge, TN 37831

Prices available from (615) 576-8401, FTS 626-8401

Available to the public from
National Technical Information Service
US Department of Commerce
5285 Port Royal Rd
Springfield, VA 22161

NTIS price codes
Printed copy: A03
Microfiche copy: A01

SAND96-1367
Unlimited Release
Printed June 1996

Distribution
Category UC-910

Near Perfect Optics

R. Goeke — Thin Films and Brazing
A.V. Farnsworth — Computational Physics & Mechanics
C.C. Neumann — Neutron Tube Development
W.C. Sweatt — Optics and Exploratory Technologies
M.E. Warren — Photonics Research
J.W. Weed — Thin Films and Brazing

Sandia National Laboratories
Albuquerque, NM 87185

Abstract

This report discusses a novel fabrication process to produce nearly perfect optics. The process utilizes vacuum deposition techniques to optimally modify polished optical substrate surfaces. The surface *figure*, i.e. contour of a polished optical element, is improved by differentially filling in the low spots on the surface using flux from a physical vapor deposition source through an appropriate mask. The process is expected to enable the manufacture of diffraction-limited optical systems for the UV, extreme UV, and soft X-ray spectral regions, which would have great impact on photolithography and astronomy. This same technique may also reduce the fabrication cost of visible region optics with aspheric surfaces.

Summary

The following images demonstrate the effectiveness of the process on our first attempt. However, our first model for generating the correction mask was overly simplistic, excluding higher order correction terms, resulting in less improvement than mathematically predicted. The figures show the aberrated optic, the corrected optic, the mathematical correction estimate, and the result of deposition through the correction mask onto a flat test plate. As seen the correction deposition closely resembles the computer caluculated correction as well as the smooth portion of the aberration; it is the bridge between the aberration and the generation of the correction which needs refinement.

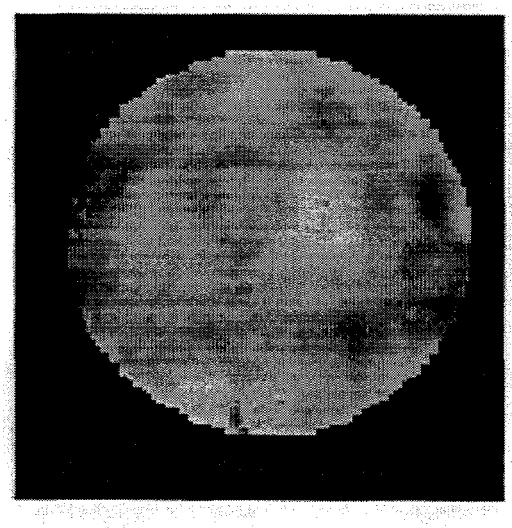

Aberrated Optic, RMS = 6.4 nm

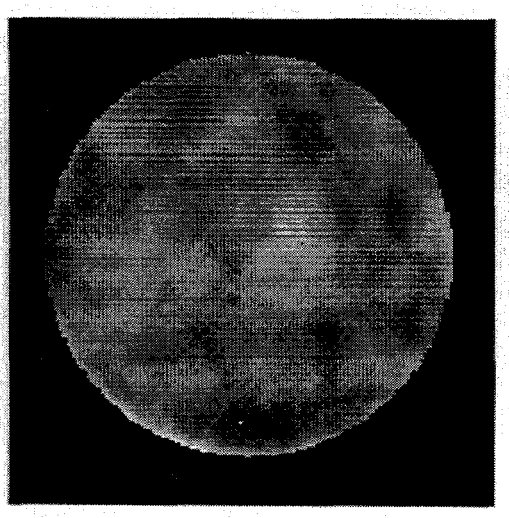

Corrected Optic, RMS = 4.1 nm

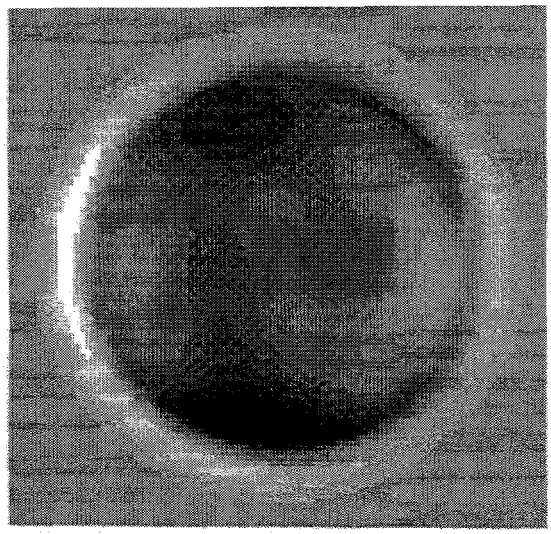

Deposition Estimate

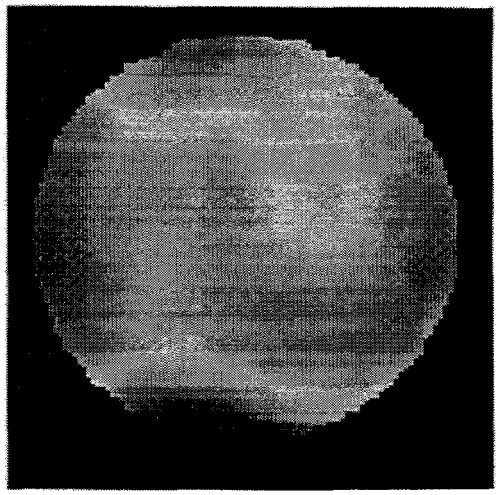

Deposition on optical flat

Acknowledgment

The authors thank A. Howard, E. Chason, Tom Mayer, and Richard Shagam of Sandia National Laboratories as well as David Merriman of Rockwell, Rocketdyne Albuquerque Operations.

Contents

Nomenclature

Figure	Surface contour; features ~ mm - cm; from polishing.
Ripple	Surface features ~ 100 microns; from mask hole spacing.
Micro-roughness	Surface roughness ~ 10nm - 5 microns ; molecular surface fill.
AFM	Atomic Force Microscopy
CRADA	Cooperative Research and Development Agreement
EUVL	Extreme Ultra-Violet Lithography
FT	Fourier Transform
FFT	Fast Fourier Transform
FWHM	Full Width Half Maximum
IR	InfraRed
LDRD	Laboratory Directed Research and Development
NPO	Near Perfect Optics
QCM	Quartz Crystal Micro-balance
RMS	Root Mean Square
SiO	Silicon Monoxide

SAND96-1367--1996
Unlimited Release
Printed June 1996

Distribution
Category UC-910

Near Perfect Optics

Introduction

The Near Perfect Optics (NPO) process uses vacuum deposition techniques to improve what are already the best optical surfaces that can be made. The surface figure is improved by differentially filling in the low spots on the surface using flux from a physical vapor deposition source through an appropriate mask. This report discusses successful correction of an optical flat; extending the demonstrated process from optical flats to aspheres, requiring minor changes in the mask design software and would give Sandia the capability of making the most accurate reflective aspheric optics in the world. It would improve both the performance of deep ultra-violet (UV) lithography tools and the resolution of deep UV telescopes, and would be an enabling technology for extreme UV projection lithography (EUVL), a current Sandia program.

Background

Industry Requirements for NPO

We have elected to focus our efforts in this project on a specific "customer" that truly needs this technology. This has given us purpose (somebody cares about our success!) and it gave us a limited set of specific goals on which to concentrate. Our chosen customer is the EUVL program which is a national program that is attempting to build a lithography tool that can produce microcircuits with 0.1 μm design rules (minimum feature sizes). They are using an all-reflective camera to image a mask onto a wafer using 13.4 nm radiation. Their camera mirrors are typically super-polished and mildly aspheric. At present, their best mirrors are produced using computer-controlled polishing with a small (sub-aperture) lap to accommodate the deviation from a sphere. With such a technique, the aspheric can be polished in, and low-spatial-frequency errors like third-order astigmatism and coma can be polished out . The resulting mirror surfaces have root-mean square (RMS) roughnesses of about 1 nm composed of mid-spatial frequency aberrations -- an unfortunate side effect of using a small polishing lap. *These are the errors the NPO technique would remedy; they are largely uncorrelated "valleys" and "hills" with heights of 1-2 nm and characteristic widths that range from 5 mm to 30 mm on a 100 mm substrate.* These specifications may be more stringent than necessary for other potential customers; however, we can always back off and solve easier problems.

Related Work

Technologies used to correct the wavefront of optical surfaces have included aforementioned sub-aperture polishing, as well as ion milling, and coating through a computer-driven, moveable mask with a single large hole. Past objectives, initially as early as 1936 and more recently in the 70's,[1] have been to develop a cheap way to make large aspheric mirrors from spheres. Relative to EUVL objectives, the shortfalls of sub-aperture polishing were described above and in fact represent what we intend to correct. Secondly, though ion milling can be used to level high spots on an optical surface, it produces unacceptably high surface roughness because of grain boundaries and sub-surface damage. Researchers elsewhere are attempting to relieve this sub-surface damage. Mild aspheres are being made commercially using coating processes similar to ours; each mask contains a

single large aperture and these apertures are designed so the deposition is heavier where the parent surface needs to be built up. This technique works well when adding a few microns of low-order spherical aberration to a surface, but it cannot be used to correct high order aberrations or mid-spatial frequency errors. Additionally, these techniques in the past have been used to make much thicker coatings than ours (hundreds of microns, in fact) which resulted in a surface too rough (RMS ~ 1% deposition thickness) to be useful for anything. Our proposed optical surface optimization process overcomes the others' shortfalls to meet EUVL objectives for the highest performance systems operating at extremely short wavelengths, far below the visible region of the electromagnetic spectrum

Near Perfect Optics Process

Process Overview

Our process for generating a near perfect optic is depicted in Figure 1. The process begins with an optic polished as near to the desired shape as possible using conventional fabrication techniques. Using interferometry, the surface error is measured which enables the design of a corrective mask for an appropriate deposition geometry. Finally the mask defines the pattern of the vacuum evaporated thin film. The resultant thin film fills in all the low spots on the surface, much like a water reservoir would over-fill a valley (see Figure 1).

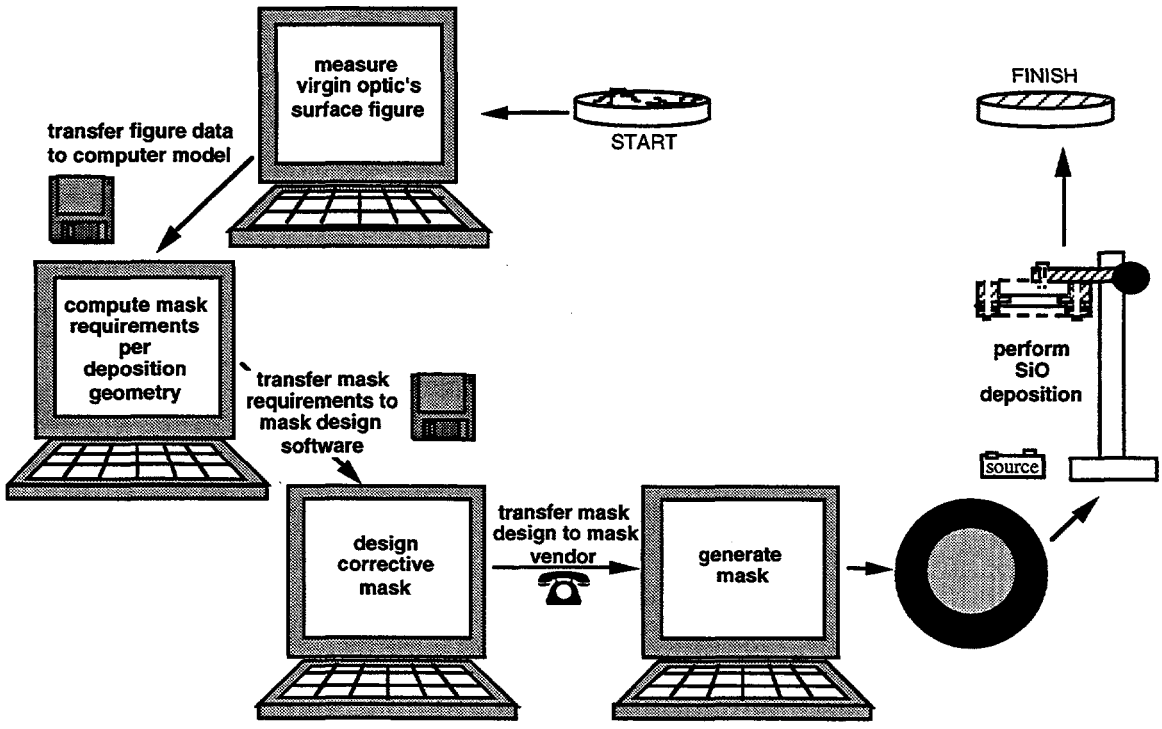

Figure 1 Near Perfect Optics Process Flow

Surface Metrology

A vendor owned-and-operated Zygo Mark IV optical interferometer, with an ultimate resolution of $\lambda/200$, was used for measurement of the optical figure of the substrates. That instrument is a computerized phase-shifting interferometer that allows computer acquisition of the optical figure information and post processing of the data, including fitting with Zernike polynomials for an approximate mathematical description of the optical surface. Surface roughness measurements were made with a Sandia owned-and-operated atomic force microscope (AFM). The AFM is a Digital Instruments Dimension 3000 operating in tapping mode that can allow surface profiling with a height resolution of less than an angstrom and a lateral resolution of ten angstroms. The data is in digital form that can be displayed as 3D surface profiles or analyzed in cross section. A vendor owned-and-operated optical surface profilometer, consisting of an automated phase-shifting interference microscope, was used for analysis of larger scale surface roughness from preliminary deposition mask experiments.

Corrective Mask Design

The deposition geometry is shown in Figure 2; the fixture controls source-to-substrate L_{ss} and mask-to-substrate, L_{ms}, separations. Depositions were performed in Sandia's Thin Film Laboratory. A mask with a square array of tiny holes is mounted, as shown, a few centimeters below the downward facing, super-polished optical surface to be corrected. The evaporation source (described in detail in Appendix A) emits a uniform flow of neutral SiO molecules that move ballistically and adhere either to the mask or pass through the holes and deposit on the surface of the optic. The spacing between centers of the holes in the square array is 100 microns. The hole diameters range from 30 to 70 microns which allows the locally averaged transmission of the mask to be varied.

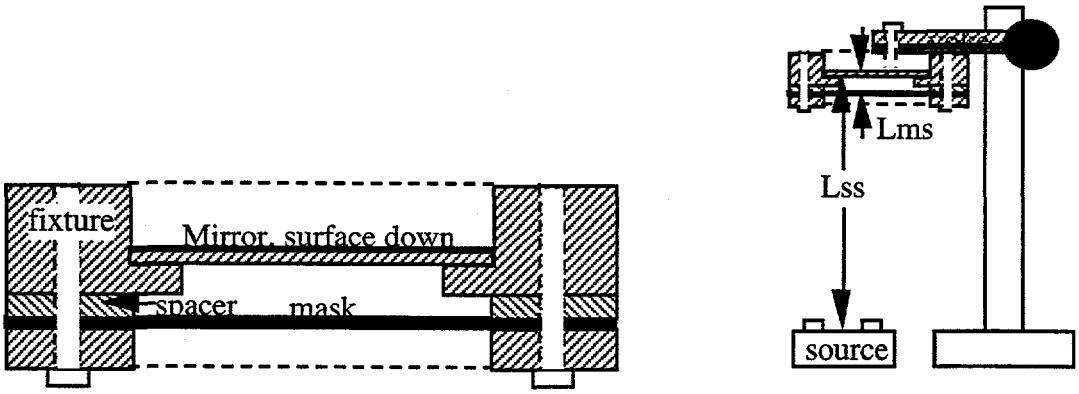

Figure 2 Mask and Fixture Geometries

Each hole in the mask acts like a pinhole camera which images the source on the optic. Typically the source has a diameter of 20 mm which creates a 2-mm image on the optic,

$$\frac{L_{ms}}{L_{ss}} = 10$$

The holes in the mask are 100 microns apart so any spot on the optic is "seeing" the source through about 300 holes. Thus there is a lot of averaging and smoothing taking place, and the concept of a local "average" transmission makes sense. Our 2-mm source image and high density hole pattern is therefore capable of differentially filling in the 5-mm to 30-mm low spots on these mirrors described under "Industry Requirements".

The deposition mask design code is based on a Fourier transform algorithm and is written in FORTRAN to run on a workstation for high performance. The output of the design code is a list of x,y hole coordinates and a hole diameter for each coordinate in a large ASCII file. The hole size can be varied from 30 to 70 microns in diameter in the design.

The upper limit is imposed by the center-to-center distance (100 microns) of the current hole array and the lower limit is imposed by the desire to limit fabrication difficulty for the mask vendor. These limits could be exceeded in either direction to meet special requirements. The large ASCII file is in turn read by a program that transfers the data to an integrated circuit CAD system. The CAD system allows addition of features for alignment or test purposes and then can output a file in a format that commercial photomask and chemical milling vendors can use. The vendor fabricates a deposition mask with the desired hole sizes by a photolithographic process combining chemical milling and electroforming. Electroforming is used to form the small holes in plated copper on a stainless steel substrate. The stainless steel behind the holes is then chemically milled away to provide a clear hole through the entire structure. This process can be used to produce holes of a few microns diameter in mask that is 75 microns thick.
Measurements of optical surface errors were received from the measurement services vendor as Zernike polynomial coefficients. A constant thickness minus this error represents the distribution of material necessary to repair the error. Derivation of the actual thickness required for repair is in the next paragraph.

Scheme for Calculating the Locally Averaged Mask Transmission

Appendix B describes the mathematics associated with the NPO coating design in detail; only the results are described here. Consider the relationship between the locally averaged transmission of the mask , $T(x,y)$, and the height of the surface error of the optic, $H(x,y)$. The 2 mm source image on the surface, $S(x,y)$, is relatively large and will blur the fine detail of the mask. Because the "information content" of the surface error, and hence the mask pattern, does not overlap in spatial frequency content with that of the mask, their effects on the deposition can be considered separately. We can calculate the local average transmission of the mask that will deposit a variable thickness layer on the optic. Mathematically, this can be described as

$$H(x,y) = \int_{-\infty}^{\infty}\int T(\alpha,\beta)\, S(x-\alpha,\, y-\beta)\, d\alpha d\beta \text{ or symbolically,}$$

$$H(x,y) = T(x,y) \ast\ast \ S(x,y)$$

where the double asterisk signifies a convolution operation in two dimensions. The transmission could be calculated from this expression, though it would be laborious, would require a number of assumptions, and would provide very little insight into the process. Ah, but we know about Fourier-transforms (FT) which translate convolution operations into simple multiplications in the spatial frequency domain. We will follow the convention of writing a FT variable in lower case, so, for example, h(p,q) is the FT of $H(x,y)$ and p and q are the spatial frequency coordinates with units of cycles/mm. The FT of the convolution witten above is,

$$h(p,q) = t(p,q) \bullet s(p,q).$$

This transformed relationship is a simple product so both sides can be divided by the source term yielding an expression for the locally averaged mask transmission,

$$t(p,q) = h(p,q) \ / \ s(p,q).$$

One dimension of these transform functions is sketched in Figure 3 and described below. Figure 3 shows three Fourier transforms of (1) the source image $s(p,q)$, (2) the 50-micron holes in a 100-micron square grid $t(p,q)$ and (3)the FT of $H(x,y)$, which describes the hills and valleys on the optic, $h(p,q)$. The divisor of the above equation, $s(p,q)$, is positive and non-zero in the lower frequencies -- the region containing the optical surface information $h(p,q)$.

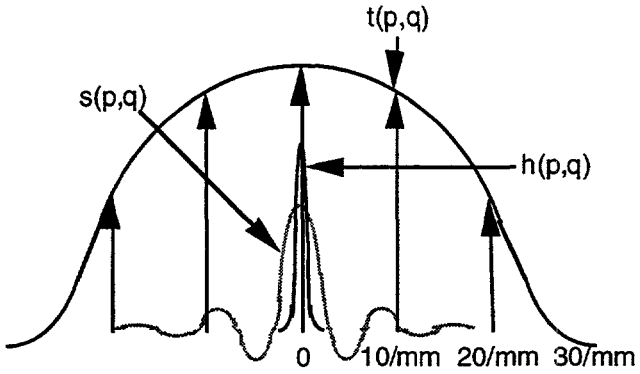

The source function in Figure 3 is the FT of a round, uniformly emitting source. It is the well known Sombrero function[ii], $somb(p,q) = J_1(2\pi\ r)/(2\pi\ r)$. The mask function, $t(p,q)$ is the wide envelope multiplied by the array of delta functions; it is described below. Also shown is an approximate frequency envelope of a typical surface with errors as small as 5mm. A summary of the FT mask design algorithm is: first, smooth the interferogram of the surface and subtract the desired aspheric shape; second, take the FT of this and divide it by the FT of the source; and finally take the inverse FT of this result which will yield the locally averaged mask transmission.

Mask Contributions to the Micro-roughness

To calculate the micro-roughness, we can assume that all of the holes have 50 micron diameters in a local region. In this region, the mask can be mathematically described as a square grid of delta functions (a 2-dimensional comb function) on 100-micron centers convolved with a 50-micron diameter cylinder function,

$$T(x,y) = comb[(x,y)/100] * * cyl[(x,y)/50].$$

And, once again, the deposition is

$$H(x,y) = T(x,y) * * S(x,y)$$

These two equations can be combined and the FT taken, giving the FT of the surface height:

$$h(p,q) = H_O\ comb[100\mu m(p,q)] \bullet Somb[50\mu m(p,q)] \bullet Somb[2000\mu m(p,q)]\ ,$$

where H_O is the average height of the deposition.

Figure 3 again shows all: the delta functions and the sombrero represent the hole pattern in the mask, and the source sombrero is in the center. Remember that the FT of the coating's micro-roughness is the product of all three functions. The delta function representing the fundamental frequency is attenuated a little (~20%) by the envelope function representing the mask holes and a lot by the source term, $s(p,q)$. As is described in Appendix B in gory detail, the sombrero representing the source can be approximated and the RMS height of the surface can be shown to be less than

$$H_{RMS} \leq 0.0072\ H_O$$

Theoretically then, if the coating thickness is never greater than 15 nm, the RMS micro-roughness will be less than $H_{RMS} \leq 0.1\ nm$. WYKO TOPO measurements on three sample depositions showed periodic errors less than this maximum.

Two other mask architectures were examined; one assumed that variable-sized holes were located on a fixed, hexagonal grid. The other was a study of fixed hole diameters with a grid that varied in one dimension. That is, all rows were separated by a fixed distance but each row had variable hole spacing in it, these variations changed from row to row. Both of these options reduced the micro-roughness but increased the cost of implementation considerably. Our decision was to use a square grid for now because of its simplicity, but to reconsider after the first series of experiments.

Thin Film Deposition

Vacuum evaporation was chosen as the deposition process because it produces an atomistic flux that is ballistic, predictable, and repeatable. The flux can then be modified by the transmission mask to produce the desired film. Silicon monoxide (SiO) was chosen as the deposition material for several reasons. Primarily SiO has a reputation for condensing as an amorphous thin film when evaporated. We believe that an amorphous material, compared to a crystalline material, will produce a film with lower residual surface roughness and will thus preserve the super polished character of the initial optic. SiO was also chosen because there are commercially-available, resistance heated, sources specifically designed for SiO evaporation. These sources have been used for many years and produce a symmetrical, molecular beam. The beam, or flux, varies in density across its radius by a cosine power function that is dependent on the geometry of the source. Once characterized at a given deposition rate the flux is easily modeled. Finally we expected that SiO would adhere well to optics made of SiO_2 or Zerodur. This technology may be extendible to other materials. For example, there are numerous exotic infrared (IR) refractive materials that are extremely difficult to polish because they are quite soft or somewhat soluble in water. We could ask the optician for a smooth surface with loose wavefront tolerances and then fix it with our technology.

The deposition system consists of standard stainless steel vacuum chamber with a cryogenic high vacuum pump. The chamber achieves pressures of 10^{-7} Torr with overnight pump-down. The evaporation apparatus includes the commercially available source, a quartz crystal micro-balance (QCM) deposition controller, and a vacuum compatible optical mount. As depicted in Figure 2, the mask and optic are loaded into the fixture which is then precisely positioned over the source with the optical mount. The source to optic distance can be varied by moving the fixture along the mount. The mask to optic distance can be varied by changing the spacer rings separating the two. A typical deposition rate is 10Å per second and is closed loop controlled by the QCM. The QCM also shuts off the flux and thus controls the film thickness.

To prepare for a deposition run the mask and optic are fixtured and the system is evacuated below 10^{-6} Torr. The evaporation source is powered with a low voltage, high current supply which heats the SiO to a temperature that produces a 10 Å per second rate at the optic's surface. The QCM controls the film deposition from start to finish. No ancillary heaters are used to heat the optic during deposition. When the run is completed, the system is vented with nitrogen and the optic removed.

Near Perfect Optics Experiments

Surface Micro-Roughness

Surface micro-roughness was measured using an atomic force microscope (AFM) and although contact and tapping modes yielded the same results, tapping mode may cause less surface damage. One of our super-polished optics was tested both before and after SiO depositions. AFM measurements of a 300 Å coating (0.17nm RMS, same as un-coated optic)[iii] imply that this may be correct -- that the SiO deposition contributes little micro-roughness. This contribution to the micro-roughness is acceptable, though a number twice this large would be worrisome for the EUVL program. We should have been able to

measure a difference if the deposition had contributed more than 1 Å RMS to the roughness. AFM surface measurements were also performed on optics which underwent ion beam annealing either during or after deposition.[iv] This operation doesn't measurably improve evaporated surface smoothness so we have not pursued this technology.

Model Verification

When depositions on optical surfaces were performed, they were compared with theoretical predictions, the expected deposition layer was calculated using a model for the source that took into account the slight variations from a simple "top-hat" flux distribution. These predictions were found to be in agreement with depositions made through special test masks, to within our ability to measure the deposited layers. The effect of the discretization of the desired transparency function by varying hole diameters in a pattern of holes in the mask is clearly seen in computed results and in the results experimentally obtained. For present purposes, this "ripple" effect can be made small in comparison to either the errors being considered, or with our ability to discern error in an optical surface, for state of the art optical surfaces.

Process Verification

Though we have had the opportunity to process only a single aberrated optic, as seen in the first figures of this document, the mask generated precisely what it was designed to produce, and the deposition process worked as expected; it is the additional detail in modeling the aberration which should be refined. This could be improved by adding spline functions to better fit the aberration data to subsequently generate higher resolution correction mask.

Conclusions

With few exceptions, the process for correcting nearly perfect optics performed as expected. One exceptions is the aforementioned resolution of the aberration model. Additionally, the fourier transform method of modeling the aberration is not as effective near the edges; modification of the formalism using some type of filter could be used to minimize such edge effects. Finally, the correction could be enhanced through improved fiducial marks for alignment of the optic with the correction mask .

Future work should include process modifications to address these exceptions to the generation of Near Perfect Optics. Review of the latest optical fabrication techniques to ensure compatibility also will be necessary; in fact, teaming with an optical fabricator to generate a complete soution aligned with current polishing techniques may be the ideal situation for proceding with this promising technique.

References

[i] R.R. Austin, J.R. Kurdock, Correction of Optical Elements by the Addition of Evaporated Films in *Physics of Thin Films*. Academic Press, NY, 1978.

[ii] J.D. Gaskill, *Linear Systems, Fourier Transforms, and Optics*, p.72, John Wiley & Sons Inc., NY 1978.

[iii] Arnold Howard, Leo Griego, *Efforts to Date on AFM Characterization for the NPO LDRD*, March 1995.

[iv] T. Mayer, private communication, February 1995.

APPENDIX A, SOURCE

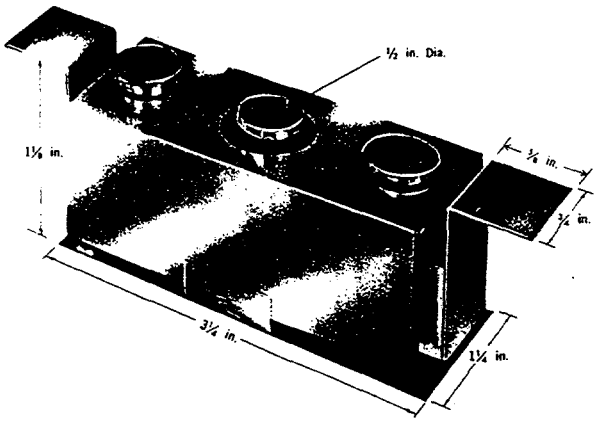

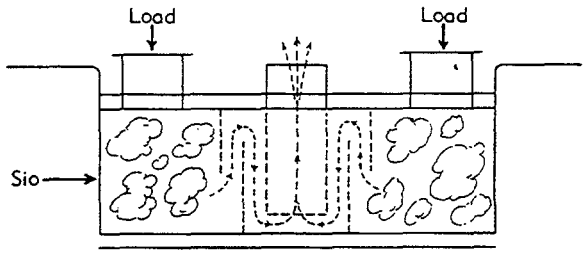

SO - 24 (UP EVAPORATION)

R.D. Mathis evaporation source/boat

APPENDIX B, MODELING

In the near-perfect optics project, we hope to reduce the wavefront errors of very good mirrors to the point that they are un-measurable. The mirrors can be polished to an RMS surface error of less than one nanometer but we need to reduce this by a factor of ten. To smooth the surface we deposit a thin coating on it using a variable transmission mask to modulate the thickness (Figure 1). With the mathematics presented here, we expect to be able to model the deposition both macroscopically and microscopically. We have made only two assumptions: 1.) The flux from the evaporative source is assumed to fill the exit aperture uniformly, and 2.) there is no significant scattering outside the source. Both assumptions seem to be borne out by our initial tests.

Figure 2 shows the important spatial frequencies associated with a mirror which may be the best medium-sized aspheric mirror in the world. Included are the mirror size, the surface defects prior to improvement, and a set of parameters describing the mask. The mirrors are about 80 mm in diameter and the spatial frequencies of the surface errors that need to be fixed are $\eta_{mirror} \leq 0.2\ mm^{-1}$. The spatial frequencies associated with the circular source exit aperture are plotted in the center of the figure. The frequencies describing the local effects due to the 2-D array of holes in the mask are quite a bit higher than those described above. The holes are located on 100-μm centers so the fundamental frequency in the "ripple" will be $\eta_{fundamental} = 10\ waves/mm$.

Note that the frequencies of the errors to be fixed and those associated with the ripple are separated by almost two orders of magnitude. Hence they can be analyzed separately. For the macroscopic problem, the mask transmission can be assumed to be smoothly varying which allows it to be calculated in a fairly straight forward manner. The ripple associated with the hole pattern can be analyzed assuming the holes are all of equal size... which will be true locally.

In the next section we present an analysis of the macroscopic problem showing how the smoothed transmission of the mask can be calculated from an interferogram of the mirror. In the following sections the ripple is studied. This gives insight about the optimum grid spacing, range of hole sizes, mask-to-substrate separation, and hole pattern-- should it be square, hexagonal, or variable? It also leads us to want the minimum average coating thickness that allows the wavefront errors to be corrected.

COMPUTING THE GLOBAL TRANSMISSION OF THE MASK

We have a mirror substrate with a wavefront error that we want to fix. This surface height error could be defined as $H(x,y)$. There are two other parameters that also need to be defined; the image of the mask transmission on the substrate, $T(x,y)$, and the source image on the substrate, $S(x,y)$. The image of the mask on the substrate is the deposition that one would get with only a point source of material rather than an extended source (Fig B3a). The source image is the deposition one would get using the real source and a mask with a vanishingly small hole in it (Fig. B3b).

With these definitions, the deposition on the surface is the convolution of them;

$$H(x,y) = T(x,y) \;**\; S(x,y). \qquad (1)$$

We know $H(x,y)$ and $S(x,y)$, and we need to determine the transmission of the mask, $T(x,y)$. It can be determined by simply deconvolving the deposition function, $H(x,y)$ though this approach gives very little insight that would help to design the process. A more instructive approach, and perhaps an easier one uses Fourier transforms to simplify the analysis. One can take the Fourier transform of the Equation (1) which changes the convolution into a simple product (See Gaskill's book). Then both sides of the equation can be divided by the transform of the source, and finally, the results must be transformed back into dimensional coordinates.

The Fourier transform of the height function, Equation (1), is thus

$$h(\alpha,\beta) = t(\alpha,\beta) \cdot s(\alpha,\beta), \qquad (2)$$

where the lower case letters denote Fourier transforms and α,β are variables with units of spatial frequency (*1/mm*). We next divide through by $S(\alpha,\beta)$ giving the transform of the mask transmission,

$$t(\alpha,\beta) = h(\alpha,\beta) / s(\alpha,\beta). \qquad (3)$$

This operation is legitimate when the transform of the source, $s(\alpha,\beta) \neq 0$, is nonzero where $h(\alpha,\beta)$ is defined. This is the case when the source image on the substrate is considerably smaller than the errors to be fixed. In our case the frequencies for the errors are smaller than $\eta_{wavefront} \leq 0.2\ mm^{-1}$ which corresponds to the spatial frequency components in 5-mm bumps and holes on the substrate. The transform of a source with $D_{source\ image} \approx 3\ mm$ is well behaved in this region; in fact, it only varies from $1 \geq s(\alpha,\beta) \geq 0.75$. From Figure B1 we can see that the 3-mm diameter seems to be a reasonable compromise between the better fidelity for fixing errors that a smaller source image would give and the lesser amount of ripple associated with a larger source. This will be shown in the next few sections.

But how do we calculate the average mask transmission? An interferogram of the surface is needed. The ones I've seen that measure to better than 1 nm have about 80 resolution elements across the diameter since they are actually composites of many raw interferograms. They show some noise so they have to be smoothed. This could be done by convolving them with a Gaussian function (or something) that has a FWHM that is a few pixels wide. As per our discussion above, this convolution might better be done in transform space where it would be a product. Given this smoothing concept, the transmission of the mask might be calculated as follows:

1. Use a commercial fast Fourier transform (FFT) routine on the interferogram data.
2. Multiply it by the smoothing function and if need be, throw away any residual noise representing spatial frequencies greater than $\eta \geq 0.2\ mm^{-1}$.

3. Divide it by the sombrero function describing the source in transform space.

4. Inverse transform this data using the FFT routine. This gives a coarse grid of data points that describe the smooth mask transmission.

5. Fit a smooth function through this data so the mask transmission can be calculated locally.

6. Calculate the hole size (or spacing) in the mask.

CALCULATING THE RIPPLE DUE TO THE PERIODIC HOLE PATTERN

Let's model one of our early experimental runs which is shown in Figure 4. It has a source diameter, $D_{source} = 12.7\ mm$, a source to mask distance, $L_{source\ to\ mask} = 200\ mm$, and a mask to substrate distance, $L_{mask\ to\ substrate} = 20\ mm$. The deposition on the substrate is a function of the geometry, the source size and shape, and the transmission function of the mask. The mask used was a square array of round holes. The grid spacing was $\Delta X = \Delta Y = 100\ \mu m$ and the hole diameter was $D_{mask} = 50\ \mu m$.

As described in the previous section, the deposition is the convolution of the source image on the substrate through a one-pinhole mask and the mask when the source is infinitesimally small. The mask image for a uniform array of holes is shown in Figure 5. The image of the source has a diameter of

$$d_{source} = D_{source} * L_{mask\ to\ substrate} / L_{source\ to\ mask}. \qquad (4)$$

The image of the mask is a bit larger than the mask itself. its magnification is

$$m_{mask} = 1 + L_{mask\ to\ substrate} / L_{source\ to\ mask}. \qquad (5)$$

In this experiment, the image of the grid pattern on the substrate will have 55-μm holes images located on 110-μm centers. The image of the source on the substrate has a 1.27 mm diameter. As a first approximation, assume that molecules of SiO exit the source uniformly over its aperture; that is, the effluent function appears to be a "top hat" function when viewed from the mask.

To simplify the math we choose the 110-μm hole spacing on the substrate be a unit length; then we scale all of the other lengths. The diameters of the mask's hole images will therefore be $d_{mask} = 0.5$ units and the size of the source image will be $d_{source} = 11.5$ units.

The deposition can be described as a convolution of the source image and a square array of holes of (locally) constant diameter;

$$H(x,y) = \{Comb(x,y) ** Cyl(r/d_{mask})\} ** Cyl(r/d_{source}). \qquad (6)$$

As with the macroscopic problem, this equation could be solved directly using numerical integration. However, more insight can be gained by studying it in the Fourier transform space.

We propose to Fourier transform this function (Eqn. 6), sort the terms, and then transform it back into spatial coordinates. The end product of this effort is a Fourier series expansion describing the ripple. The fundamental term in this series has a period equal to the hole spacing in the mask image, $\_x = 110\ \mu m$.

The Fourier transform of Equation (6) is

$$\{H(x,y)\} = Comb(\alpha,\beta) \cdot Somb(D_{mask}\rho) \cdot Somb(D_{source}\rho). \qquad (7)$$

The spatial frequency coordinates, α and β have units of mm^{-1}. The radially symmetric coordinate is $\rho = \sqrt{(\alpha^2+\beta^2)}$.

The transform of a comb function is another comb function; recall that a comb function is an infinite set of equally spaced delta functions. The transforms of the cylinder functions are defined by Gaskill as "sombrero" functions, $\mathcal{F}\{cyl(r/D)\} = somb(D\rho) = J_1(\pi D\rho)/(\pi D\rho)$, where J_1 is a Bessel function of the first kind. These functions are drawn in Figure B4 for the parameters given.

The transform of the deposition, $H(x,y)$, is therefore the array of delta functions multiplied by a set of constants. The constant for a given delta function, $\delta(\alpha-\alpha_o,\beta-\beta_o)$, is equal to the product of the two sombrero functions evaluated at $\alpha=\alpha_o$, $\beta=\beta_o$.

We choose to associate pairs of delta functions $\delta\delta(\alpha_o,\beta_o) = \delta(\alpha-\alpha_o,\beta-\beta_o) + \delta(\alpha+\alpha_o,\beta+\beta_o)$ in the transform space. When one of these pairs is transformed back into spatial coordinates (x,y), it becomes $F(x,y) = cos[2\pi x\cdot\alpha_o)] \cdot cos[2\pi y\cdot\beta_o)]$. This is simply one of the terms in the Fourier series describing the ripple. These Fourier terms are multiplied by constants which are simply the product of the two sombrero functions evaluated at the delta function's position.

The argument of the second Sombrero function is large when $\rho \geq 1$, so this function can be approximated by the asymptotic expansion

$$Somb(\rho * D_{source}) \approx \sqrt{2}/[\pi^2 D_{source}^{1.5}]\rho^{-1.5}cos(D_{source}\pi\rho+0.75\pi). \quad (8)$$

This function can change significantly with small changes in the source diameter or magnification, $L_{mask\text{-}to\text{-}wafer}/L_{source\text{-}to\text{-}mask}$ (Eqn. 5). Hence, analyzing specific cases could be misleading. It is safer to calculate the maximum possible ripple using the envelope function,

$$|Somb(D_{source}\rho)| \leq 0.14\,(D_{source}\rho)^{-1.5}. \quad (9)$$

We now have all of the pieces of the solution so we can do the inverse Fourier transform and calculate the ripple. We use Equation (9) to represent the source instead of a sombrero function so our result will give a conservative estimate of the ripple. The sombrero function representing an average sized hole in the mask has a value of 0.72 for the fundamental terms in the ripple. Since the other terms are considerably smaller, we can estimate the maximum possible value of the first two terms in the Fourier series. This should give a conservative estimate of the surface height;

$$H(x,y) - H_0 = 0.28H_0(D_{source})^{-1.5}[cos(2\pi x)+cos(2\pi y)]. \quad (10)$$

Thus for this experiment we have an RMS surface roughness less than

$$H_{RMS} \leq 0.28\cdot D_{source}^{-1.5} H_o = 0.0072\cdot H_o. \quad (11)$$

In the following section we use this result plus the optical smoothness requirements and the mask fabrication tolerances to design the mask. We calculate an optimum grid spacing on the mask, the range of hole sizes in it, and the average depth of the deposition, H_o.

RESOLUTION AND MAXIMUM ERROR

This technology will be useful for any deep-UV or extreme-UV program. This includes astronomical satellites, lithography, microscopy, etc. It will also be useful for making extremely accurate reference surfaces for interferometry. To keep the program's goals focused, we need to choose one customer and satisfy his current needs. The Sandia/AT&T

extreme-UV lithography program is active now and has a pressing need for better optics. We feel that if we can help them, we will have solved the near-perfect problem for the other potential customers listed.

Sandia's EUV lithography CRADA partners at Bell Labs had four vendors make mirror M2 for their large format technology demonstration lithography camera. The best of these four may be the best medium-sized (62-mm diameter), aspheric mirror in the world. It has a peak-to-peak surface departure from the desired aspheric shape that is slightly larger than 1 nm. The other mirrors in this camera will be larger than M2 so we estimate that a worst case error may be in the range of 3-nm surface error. We (arbitrarily) choose this to be the maximum difference in deposition depth required.

How accurately do we have to correct the surface so it can be used at extreme UV wavelengths ($\lambda_{EUV} = 13.4\ nm$)? That is, what should the minimum change in deposition depth be? To answer this question we could assume a large area that is low by half of the minimum step. What would its effect be on the Strehl ratio? Perhaps we could allow a 0.5% reduction in the Strehl. This implies an RMS wavefront error of 0.01125 λ = 0.151 nm, which is equal to the average allowable step size. If this is divided into the maximum deposition depth, we find that 20 equal steps are required; or more if the steps are unequal.

There are two cases of interest: 1.) fixed grid with varying hole sizes and 2.) fixed hole size with a varying grid spacing.

If the grid is fixed and the hole size varies, then the minimum change in the area of the hole dictates the minimum step height change in the deposition. Mial Warren says his mask vendor has a resolution of 1 micron so the minimum change in the diameter of a hole is 1 micron. The worst-case area change is thus

$$A = \pi D_{max} \cdot 1\ \mu m.$$

A problem: The diameters of the holes should not vary over a huge range since the etching step in the mask fabrication is not totally predictable. Perhaps a range of diameters of 1:2 is reasonable? Then the maximum hole diameter is

$$20*A = \pi/4 \cdot D_{max}^{2} \cdot 0.75,$$

so

$$D_{max} = 107\ \mu m$$

and

$$D_{min} = 53\ \mu m.$$

For this hole diameter the grid size will have to be greater than

$$x \geq 150\ \mu m.$$

The range of hole diameters gives the range in the average transmission; that is, it ranges from $0.25T_{max}$ to T_{max}. The errors to be corrected are equal to 3 nm so the maximum difference in deposition depth needs to be H_{max}-H_{min} = 3 nm, which means H_{max} = 4 nm.

How much ripple might this hole pattern create? If the grid pattern is a 150-µm square grid and the source image on the surface has a 1.27-mm diameter, the ripple will be a sinusoid with a multiplier of $H_{RMS} \leq 0.013H_o = .05\ nm$ which is a bit smaller than an atomic diameter... which is acceptable.

VARYING THE HOLE POSITIONS RATHER THAN THE DIAMETERS

The holes can all have the same diameter if the grid spacing is allowed to vary. This design would not be too hard to implement if the spacing in the x direction were held constant and only the spacing in y were varied. For example, we could have a grid with a 100-μm spacing in x, and 50-μm diameter hole size, and a spacing in the y direction that varies from 75 μm to 150 μm. This mask would have a transmission that varies by as much as 2:1 with 75 different levels.

The ripple in the y direction is set by the 100-μm grid spacing. The ripple in the x direction can be reduced to near zero. This can be done by choosing the location of the first hole in each row with a random number generator. As a result, the holes don't line up into columns so the effects of their locally periodic spacings add randomly.

RIPPLE IN A HEXAGONAL ARRAY OF HOLES

A hexagonal array of holes reduces the scatter due to ripple to about 25% of the value of an equivalent square array. If the principle dimension of a hexagonal array is unity, then the transmission for the surface can be written as

$$T(x,y) = \{comb[x,y/1.732]+comb[x-0.5,(y-0.866)/1.732]\} * cyl(r/D_{mask})$$

The Fourier transform of this is

$$t(\alpha,\beta) = [1+(-1)^{m+n}]\cdot\delta(m\alpha)\cdot\delta(1.732n\beta)\cdot somb(D_{mask}\rho).$$

As can be seen, half of the terms are zero including the fundamental terms. The first few terms in the Fourier series giving the ripple are

$$H(x,y) = C_{0,0} + C_{2,0}cos(2\pi x/0.5) + C_{0,2}cos(2\pi y/0.866)$$

$$+ C_{1,1}cos(2\pi x)cos(2\pi y/1.732), \text{ etc.}$$

These Fourier components all have higher spatial frequencies than those in a square array with unit spacings. The sombrero functions that are multiplied by $t(\alpha,\beta)$ decrease rapidly for large values of $\rho = \sqrt{(\alpha^2+\beta^2)}$. Hence the constants $C_{2,0}$, $C_{0,2}$, $C_{1,1}$, etc. are significantly smaller than those for a square array. In fact, the scattered light should be about 25% as large as for an equivalent square array.

SUMMARY OF MASK DESIGN TRADE-OFFS

Requirements and Limitations: We need to be able to deposit coatings with a maximum difference in depth of about 3 nm. The coatings need a thickness resolution of about 0.15 nm to keep the scatter in a reasonable range. The features on the masks can be made with a 1-μm accuracy.

Varying the Mask Transmission: If the grid spacing in the mask is to be fixed and the hole diameter is to vary to give the coating thickness variations, then the coating must be quite thin. As stated above, the thickness needs to vary from $1\ nm \le H(x,y)-H_o \le 4\ nm$. This may not be possible if the coating exhibits "island growth". However, the good news is that the ripple is minuscule. To give the 0.15-nm surface height accuracy, the holes must vary from 53 μm to 107 μm in diameter. This implies a grid size of about 150 μm.

A fixed hole diameter with a variable grid spacing offers a greater choice of coating thickness ranges. The resolution and range can be had with average coating thicknesses of up to 15 nm. The ripple resulting from this hole pattern and coating thickness is still small. A reasonable choice of hole diameter is 55 μm with a 100-μm average hole spacing.

First Order Parameters for Deposition: Our current system has a 12.7-mm diameter source of SiO. The source-to-surface distance is about 220 mm. We need to keep the image of the source on the surface (as seen through one pinhole in the mask) in a range of 1.27-mm to 2-mm in diameter... so the mask to surface distance should be in the range 20 mm to 30 mm.

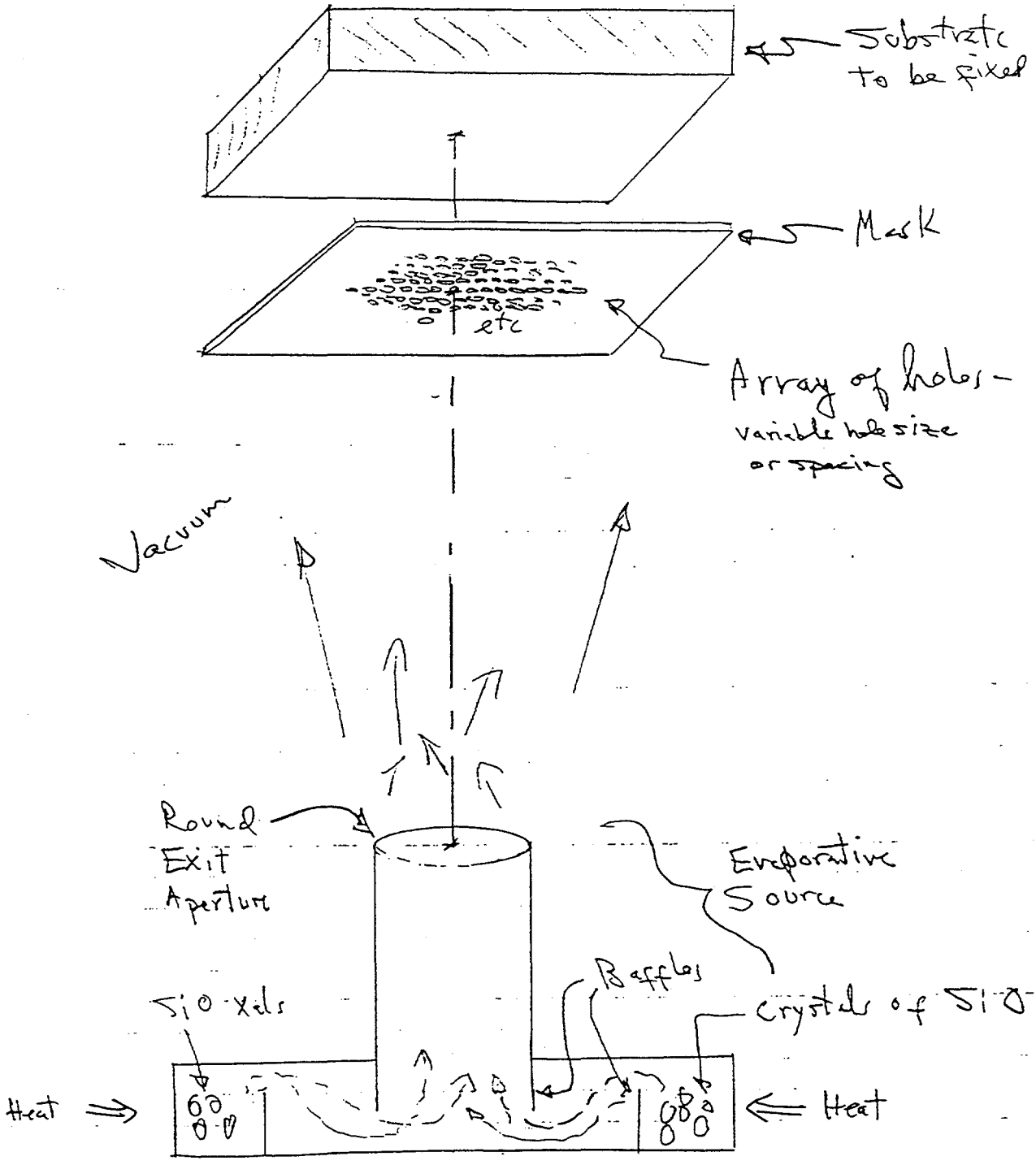

Figure B1 Source, Mask, and Substrate

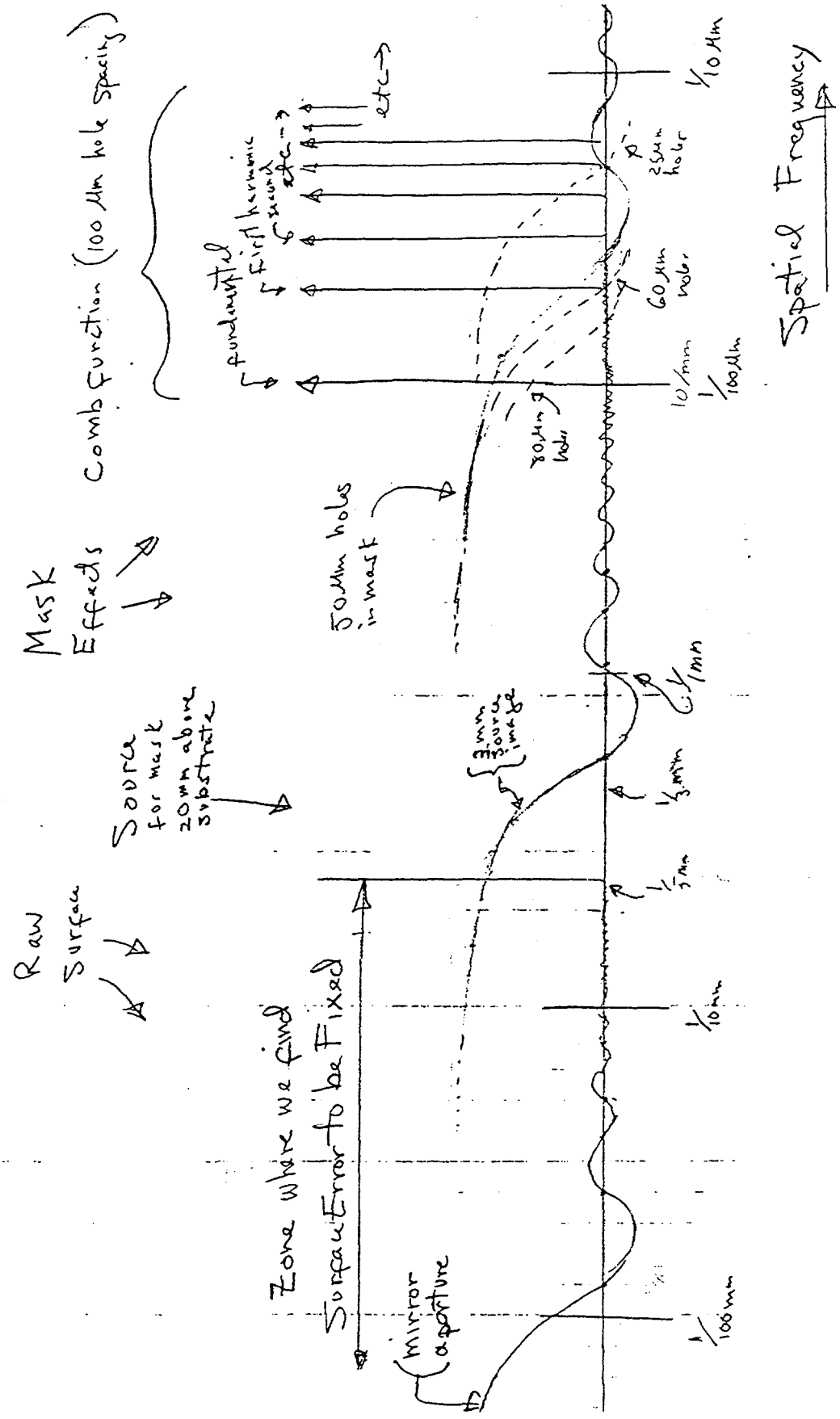

Figure B2 Spatial Frequency of Mirror Surface, Mask, and Source

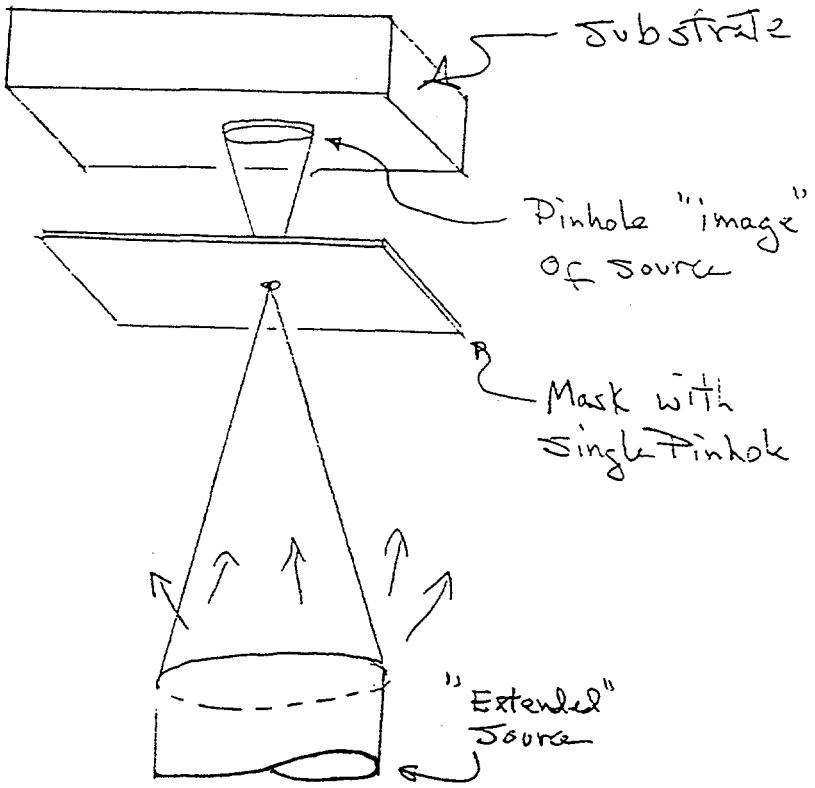

Figure B3a Definition of Source Image S(x,y)

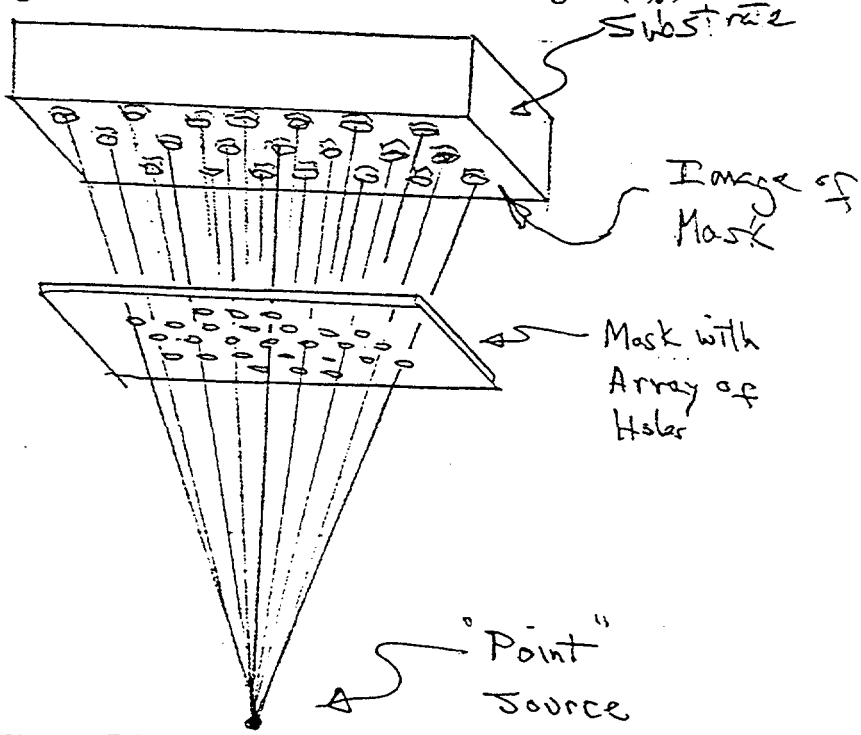

Figure B3b Definition of Mask Image T(x,y)

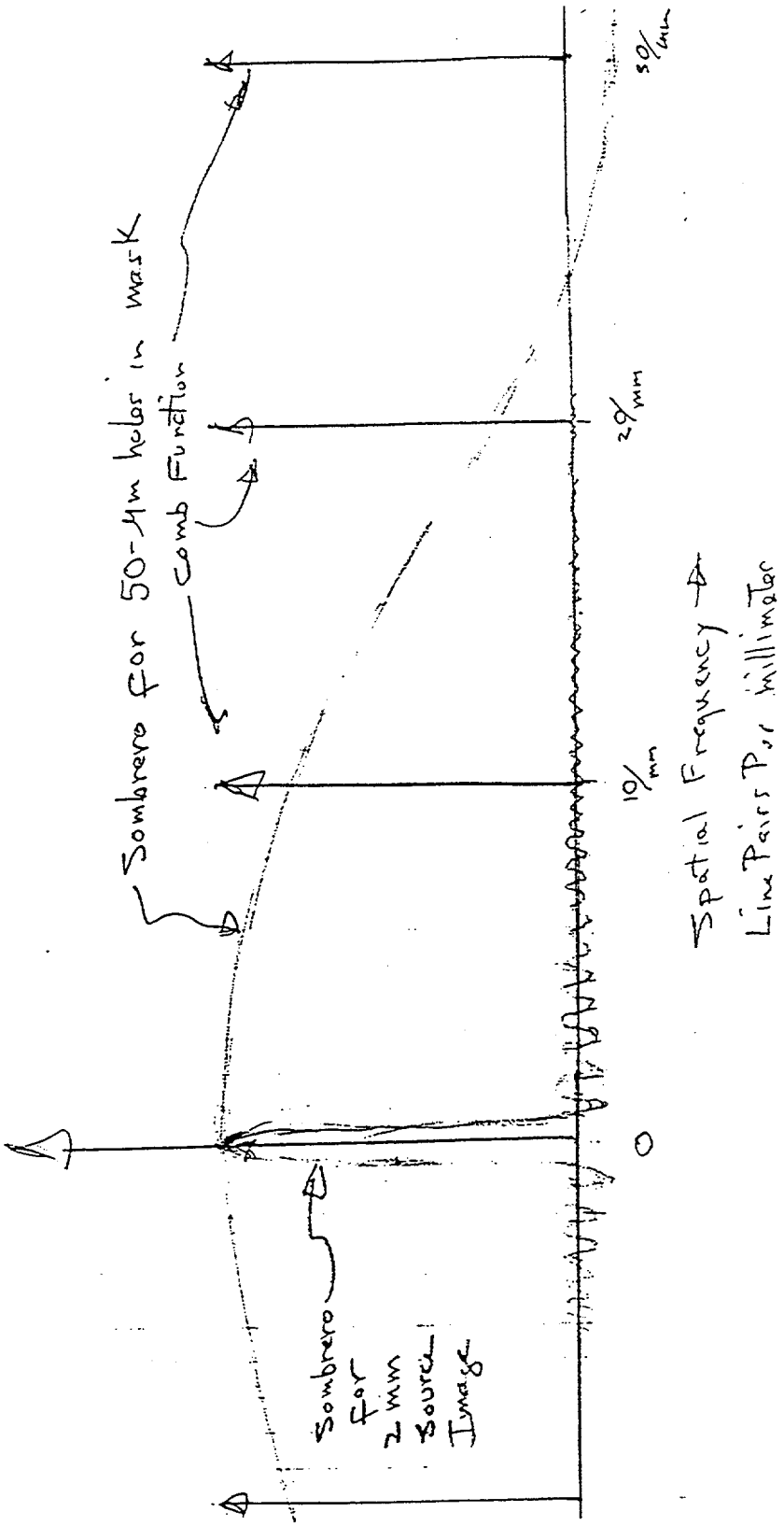

Figure B4 Fourier Transform for Square Grid of Holes in Mask

APPENDIX C, DITHERING THE SOURCE

What is proposed in the previous sections assumes that we can use a coating that varies from $1\ nm \le H_{coating} \le 4\ nm$. Evaporative coatings may not be uniform when they are this thin. One solution to this problem may be to deposit a uniform coating with the mask removed either before or after the variable thickness layer is deposited. Another solution is to use large holes and a thick layer and then dithering the source (or mask) to reduce the ripple that would have resulted.

The discontinuity at the edge of the cylinder function gives the ringing in its Fourier transform. If the edge were smoothed, the ringing could be greatly reduced. This could be done by "dithering" the source; that is, moving it around in some pattern during the deposition. The edge of the time-integrated source might therefore be softened. The question is, what should the pattern be, and how large should it be?

We propose to look at two cases first: 1.) The source motion could "paint" a gaussian distribution and 2.) it could be just moved in a circle. The gaussian motion would make the source appear as

$$S_{gaus}(r) = Cyl(r/D_{source})**Gaus(r/\sigma)$$

where $Gaus(r/\sigma) = exp[-\pi(r/\sigma)^2]$. The Fourier transform of this source would be

$$\{S_{gaus}(r)\} = Somb(D_{source}\rho)\cdot Gaus(\sigma\rho).$$

If the source motion has a gaussian radius of about one period of the grating, $\sigma = 1$, then at $\rho = 1$ the gaussian will be small; $Gaus(1) = 0.043...$ so the ripple will be 23 times smaller than the undithered case.

When the source is moved around in a circle, the time-averaged deposition would be

$$S_{circle}(r) = Cyl(r/D_{source})**\{Cyl[r/(D_{ring}+\delta)]-Cyl[r/(D_{ring}-\delta)]\}/(2\delta).$$

for $\delta \rightarrow 0$. Taking the Fourier transform of this mess yields

$$\{S_{circle}(r)\} = Somb(D_{source}\rho) \cdot [J_0(x)/x - 2J_1(x)/x^2]$$

where $x = D_{ring}\rho$. Note that the transform of the ring does not become small until x becomes large, and then it approaches an asymptotic solution with an envelope identical to that of the sombrero function. Hence, the circular motion of the source image on the substrate would have to be large (5x?) relative to grid image.

Two other possible motions-- one uniformly fill a cylinder, that is, uniform dwell time per unit area; and the other paints a conical function where the dwell time reduces linearly with radius. The sources for these two time-averaged sources are

$$S_{cyl\text{-}motion} = Cyl(r/D_{source})**Cyl(r/D_{cyl\text{-}motion})$$

and approximately

$$S_{cone\text{-}motion} \approx Cyl(r/D_{source})**[Cyl(2r/D_{cone\text{-}motion})**Cyl(2r/D_{cone\text{-}motion})]$$

The Fourier transforms for these two functions are

$$\{S_{cyl\text{-}motion}\} = Somb(D_{source}\rho)\cdot Somb(D_{cyl\text{-}motion}\rho)$$

and

$$\{S_{cone\text{-}motion}\} = Somb(D_{source}\rho)\cdot[Somb(D_{cone\text{-}motion}\rho/2)]^2$$

Both of these new sombrero functions decrease proportional to the argument raised to the 1.5 power. A sombrero function rings; it has maxima and minima that reach -13%, 6%, -4%, etc. Therefore the cylindrical motion needs a diameter greater than $D_{cyl\text{-}motion} \geq 2.2$ to achieve a reduction of the ripple to less than 4% of the fixed-source value. The Fourier transform of the cone motion is equal to a sombrero function squared, but the argument is smaller. Therefore, a cone diameter greater than $D_{cone\text{-}motion} \geq 2.4$ reduces the ripple by $[13\%]^2$, which reduces the ripple to 1.75% of the unmoved value.

DISTRIBUTION

Number of Copies	MailStop	Recipient
5	0959	Ron Goeke, author
5	0959	Woody Weed, author
5	0516	Carla C. Neumann, author
25	0980	William Sweatt, author
5	0603	Mial Warren, author
5	0820	Archie Farnsworth, author
1	1436	Donna Chavez, LDRD
1	0161	Andrew Abeyta, legal
1	9018	Central Technical Files, org. 8523-2
5	0899	Technical Library, org. 4414
2	0619	Reveiw&Approval Desk, 12630 for DOE/OSTI